Conjugated Heat Transfer of the stator of a synchronous electrical machine

Augusto Salomão Bornschlegell[1], Thiago Antonini Alves[2], Gerson Bessa Gibelli[1]

[1]*Faculty of Engineering FAEN, University of Grande Dourados UFGD*
Cidade Universitária, Unidade 2, Caixa Postal: 364, CEP: 79.804-970, Dourados - MS, Brazil
augustosalomao@ufgd.edu.br, gersongibelli@ufgd.edu.br
[2]*Dept. of Mechnical Engineering, Federal Technological University of Paraná*
Av. Monteiro Lobato, s/n km 04 Jardim Carvalho, CEP 85016-204, Ponta Grossa - PR, Brazil
antonini@utfpr.edu.br

Abstract. Electrical energy generation in remote islands and ships are mainly due the energy conversion from chemical to mechanical by an engine and converted from mechanical to electrical by an alternator. The losses in the alternator during the energy conversion are responsible for the increase of its temperature. The present work numerically evaluates the heat dissipation in the stator of an electrical machine and its maximum temperature levels. In order to reduce computational costs, due geometrical symmetry, just 1/120 of the machine was modeled. In addition to symmetry, the momentum boundary conditions consist in inlet, outlet and noslip at the walls and the thermal boundary conditions consist in imposed heat fluxes. The model is time dependent. The geometry was constructed using Salome-Meca software and the mesh was generated using the snappyHexMesh solver from OpenFOAM v11. The foamMultiRun solver from OpenFOAM was employed. The numerical schemes selected were linearUpwind second order scheme for the advective terms, Gauss first order scheme for the diffusive terms and backward second order scheme for time integration. The fluid flow regime was laminar. The model predicted the temperature distribution at the stator. The correlation between the temperature and flow fields were discussed.

Keywords: Electrical machine, Conjugated heat transfer, OpenFOAM.

1 Introduction

Electrical machines have an important role in energy conversion at remote sites such as islands and in ships. During the conversion of mechanical energy to electrical energy, losses are present, in which affect the electrical machine overall efficiency. These losses are responsible for the increase of the electrical machine's temperature, which cannot overpass its electrical insulation working class limit. The selection of the electrical insulation then defines the project temperature limit. In addition to the electrical insulation, overheat is the main challenge in the development of more compact and inovating electrical machines.

The thermal behavior of an electrical machine is usually modelled using the lumped method, as observed in Arumugam et al. [1], Eme et al. [2], Ghahfarokhi et al. [3], Khlissa et al. [4] and Kolondzovski et al. [5]. The method is based on the evaluation of the conductances of the discretized domain, considering mainly conduction and convection phenomena. The conductance of conduction depends on the geometry and on the material thermo-physical properties. It has a straightforward estimate with good precision. Convection, by the other hand, relies on experimental correlations for the heat transfer coefficient of convection with important uncertainties that can bring difficulties for the model validation. Nevertheless, the method presents a very low computational cost and acceptable temperature field predictions, which makes it an interesting tool for optimization purposes, as detailed in Bornschlegell et al. [6].

Recent technological solutions to maintain the electrical machines at low temperatures levels consisted in Heat Pipes (Wrobel and MGlen [7], Ušakovs et al. [8] and Wrobel [9]) or in Thermoelectric Electric Cooler (TEC) (Lucas et al. [10]). The later consumes electrical energy and then, it has some impact on the overall machine efficiency. Regarding the manufacture process, the additive manufacturing feasibility is explored in Selema et al. [11], Selema et al. [12], Kareem and Michael [13], Wang et al. [14] and Tiismus et al. [15]. In Chow et al. [16], there is a review of high temperature superconducting materials in electrical machines. These materials allow more compact machines. All these innovations can be better exploited when we understand the fluid behavior inside of

the electrical machine. In that sense, Kolondzovski et al. [5] use CFD to estimate the fluid flow behavior in an low cost axisymmetrical model and, then, the fluid behavior is used to estimate the heat convection coefficient which will be the boundary conditions of the full geometry conduction thermal model.

From the presented bibliography, there are few works that pay attention to the flow behavior in electrical machines. One reason is that its computational cost is prohibitive. Then, the main objective of this work is to evaluate the fluid flow behavior and heat transfer in a sequence of bifurcations that represents the cooling system of the stator of a synchronous electrical machine. This can be achieved using symmetry boundary condition at the orthoradial direction.

2 Numerical model

2.1 Geometry, boundary conditions and heat sources

The stator has geometrical symmetry at the orthoradial direction. The windings geometry repeats every 1.5 degree in the orthoradial direction. This geometrical feature is used to simplify the numerical domain and reduce computational cost. The angle of 3 degrees is considered in order to model one entire radial channel. The inlet fluid flow is positioned at the rotor-stator air gap h and the outlet is placed at the outer axial channel, above the stator, otherwise the fluid would flow straight through the air gap. This geometrical setup cools the windings, which are made of copper and the stator which is made of steel. In order to isolate the influence of the inlet and outlet boundaries, they were positioned at least 10 times their height from the stator. The geometry and boundary conditions are illustrated in Fig. 1.

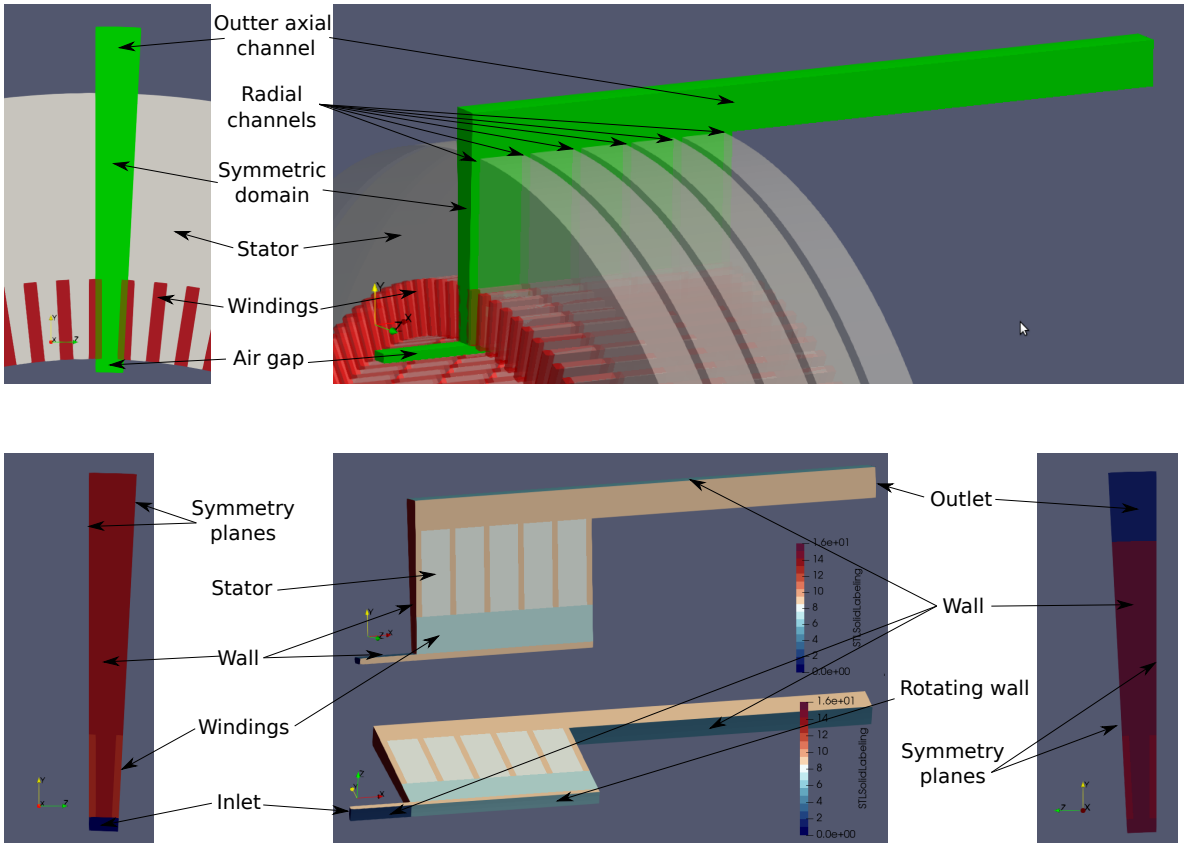

Figure 1. Domain and boundary conditions

At the inlet, it is imposed a velocity of 1 m/s which leads a Reynolds Number ($Re = \rho V h/\mu$) of 1000, where ρ is the fluid density, V the fluid velocity at the inlet and μ the fluid dynamic viscosity. The inlet and outlet channels have noslip boundary condition in the radial direction. At the interface with the rotor, at $r = R_1$, the rotational velocity of Ω is imposed so that the Rotational Reynolds Number ($Re_\Omega = \rho \Omega R_1^2/\mu$) is 1000. The noslip

boundary condition is also imposed on the remaining walls at the stator and windings. The boundary condition of symmetry is applied at the symmetry planes.

Regarding the thermal problem, the domain is considered insulated. At the inlet, the air flow enters at 300 K. Heat is generated at the windings (500 W) and at the stator (100 W) and it is evacuated to the outlet by the air flow. Since the windings are in contact with the stator, they exchange thermal energy by conduction and both exchange thermal energy with the air flow by convection. The initial conditions are fluid at rest ($\mathbf{V} = 0\ m/s$) and the initial temperature of $300\ K$ for both fluid and solid domains.

2.2 Mesh and mesh sensibility

The numerical domain was created using the blockMesh and snappyHexMesh utilities from OpenFOAM v11. The interfaces between solid-fluid and solid-solid as well as the 17 different boundaries of the geometry were designed in the Salome-Meca v2022 and exported to OpenFOAM in stl files.

The base mesh constructed with the blockMesh utility had equilateral hexahedron cells with edges of $h/2$ tall. Using the snappyHexMesh utility, the initial coarse mesh (M3) was built with refinement level 2 for all the wall surfaces. Further refinement consisted in increasing the walls refinement level. Thus, the intermediate mesh (M2) was built with wall refinement level 3 and the finer mesh (M1) with refinement level 4. An additional mesh M0 with wall refinement level 5 was necessary to achieve convergence. An ilustration of the mesh refinement at the fisrt two bifurcations from the inlet is presented in Fig. 2.

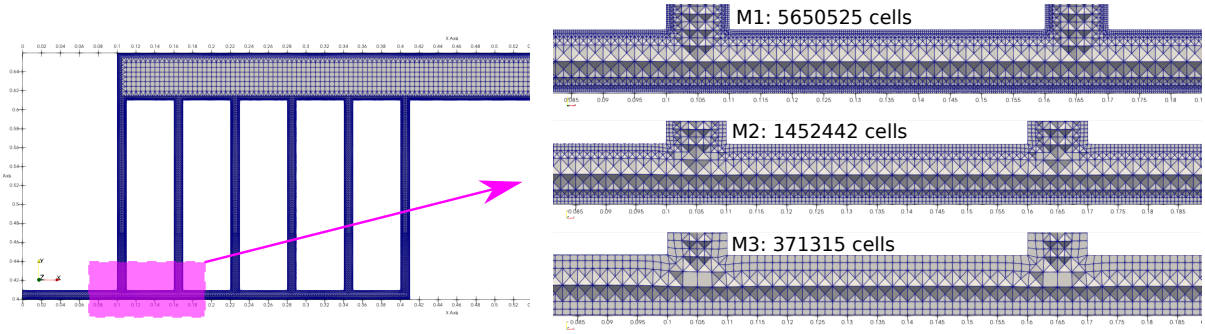

Figure 2. Mesh refinement

The mesh refinement was evaluated according to Celik et al. [17]. The ratio between the cell sizes of the different meshes was about $r = 1.6$. The interpolation order obtained for M3, M2 and M1 was $p = 1.35$ and for M2, M1 and M0 was $p = 3.62$. The velocity profiles of mesh M0, M1 and M2 are alike, then, the selected criteria was the maximum windings temperature. From Table 1, it is observed that the meshing methodology led to models with high computational cost. So, the snappyHexMesh mesher should be avoided in this kind of problem. The M1 mesh results were used in the discussion of the present work.

Table 1. Mesh independence test

Mesh	Cells	Skewness (max)	r	Tmax [K]	GCI
M0	22,772,476	1.00	1.59	320.8	0.3 %
M1	5,650,525	2.95	1.57	324.2	8.15 %
M2	1,452,442	3.43	1.57	341.5	14.06 %
M3	371,315	2.84	n.a.	373	n.a.

2.3 Thermophysical properties

The air is modeled as a pure mixture considering the specific heat of $cp = 1006\ \frac{J}{kgK}$, dynamic viscosity of $\mu = 1e-5\ Pa.s$, Prantdl Number of $Pr = 0.7$ and, for the Boussinesq approximation $\rho = \rho_0 * [1 - \beta * (T - T_0)]$, it was considered $\rho_0 = 1,0\ \frac{kg}{m^3}$, $T_0 = 300\ K$, $\beta = 3e-3\ \frac{1}{K}$.

The windings are made mainly of copper. The considered physical properties are specific mass of $\rho =$

8930 $\frac{kg}{m^3}$, thermal conductivity of $k = 400\frac{W}{m.K}$ and specific heat at constant volume $cv = 374\ \frac{J}{kg.K}$. The stator is made of steel. The corresponding properties are specific mass of $\rho = 8000\ \frac{kg}{m^3}$, thermal conductivity of $k = 50\frac{W}{m.K}$ and specific heat at constant volume $cv = 450\ \frac{J}{kg.K}$.

2.4 Numerical schemes

The multiRegion solver was employed in this simulation. It solves the Navier-Stokes equations in the 3 directions (x, y and z), described in eq. (1), using the previous time step temperature. Then, it solves the enthalpy balance equation combined with the moment balance equation, eq. (2), initially evaluating for the fluid domain and then evaluating the solid domains (stator and windings). This sequence of events makes the solution of the fluid domain as boundary conditions for the solid domain. In order to maintain physical consistency, at the solid-fluid interface, in any particular point, the temperature is the same for both fluid and solid domains as well as the heat flux (with opposing signs). The pressure correction and the continuity, eq. (3), are solved through the pressure-velocity algorithm.

$$\frac{\partial \rho u_i}{\partial t} + \frac{\partial}{\partial x_j}(\rho u_{rj} u_i) = -\frac{\partial p_{rgh}}{\partial x_i} - \frac{\partial \rho g x_j}{\partial x_i} + \frac{\partial \tau_{ij}}{\partial x_j}. \tag{1}$$

$$\frac{\partial \rho h}{\partial t} + \frac{\partial}{\partial x_j}(\rho u_j h) + \frac{\partial \rho k}{\partial t} + \frac{\partial}{\partial x_j}(\rho u_j k) = -\frac{\partial q_i}{\partial x_i} + \rho r + \frac{\partial p}{\partial t} - \rho g_j u_j + \frac{\partial \tau_{ij} u_i}{\partial x_j}. \tag{2}$$

$$\frac{\partial \rho}{\partial t} + \frac{\partial \rho u_i}{\partial x_j} = 0. \tag{3}$$

The problem was modeled as time dependent and the backward second order integration scheme was used. The maximum Courant Number was set to $Co_{max} = 1$. The Boussinesq approximation was used to estimate the air density in function of the temperature. The flow regime is laminar. The advective terms were modeled using linearUpwind second order OpenFoam implementation and the pressure-velocity coupling was modeled using PIMPLE OpenFOAM implementation, which consists of hybrid method based on PISO and SIMPLE algorithms, as detailed in Greenshields and Weller [18].

3 Results and discussion

3.1 Fluid flow

In the present geometrical configuration, the inlet volume flow rate is divided to the six vertical channels. A fluid particle at the inlet goes to one of the six vertical channels depending on its radial position at the inlet. The closer to the inner radius, the further the particle is advected at the rotor-stator air gap channel.

The velocity profiles of each component (Ux, Uy and Uz) at different positions in the rotor-stator air gap are present in Fig. 3. At the walls, the nonslip boundary condition is verified with $\mathbf{V} = 0\ m/s$, except for the Uz profile at the inner radius (R1), where the rotational speed is imposed. For the axial direction (Ux), the parabolic profile is observed at the first radial channel entrance ($x = 0.100\ m$). Since the radial channels draw the air gap flow, the profiles from $x = 0.110$ on have their maximum magnitudes above the middle of the channel. For the same reason, the same behavior is observed for all the Uy profiles, but at lower order of magnitude. Indeed, the secondary flow (Uy and Uz) has maximum magnitudes of 0.2 m/s whereas the main flow (Ux) has maximum magnitude of 1.3 m/s. A recirculation region at the end of the rotor-stator air gap can be observed at $x = 0.400m$ of the Uz profile.

The Uy velocity profile along the 6 radial channels of the stator, from left to right, are illustrated in Fig. 3. The flows along the channels are characterized by high velocity magnitudes at the right side of the channel. At the left side of the channels, there is a recirculation region (negative values) in the first 5 channels. This effect is not observed at the last channel. The maximum positive values are observed at 25 mm from its beginning. As the fluid flow through the radial channel, momentum diffusion spreads de velocity profile. There is a geometrical abrupt change of the cross section, after $l = 0.050\ m$, where the flow loose contact with the windings at the orthoradial direction. The mean velocity is also affected by the decrease of the cross section.

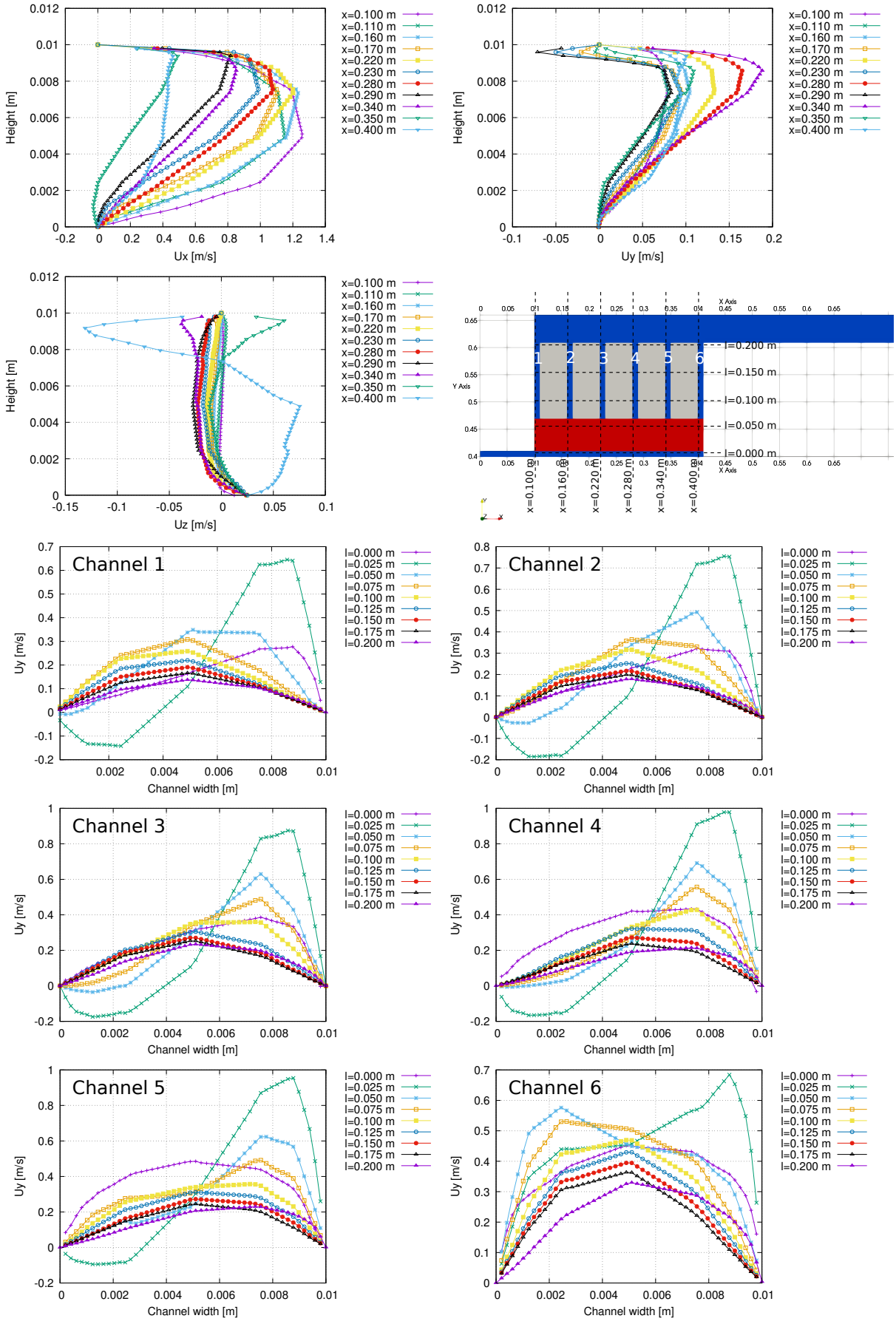

Figure 3. Velocity profiles at the air gap and stator channels

At the stator outer axial channel, the mean flow magnitude increases with the contributions of the vertical channels. Since the outer axial channel is 5 times greater than the air gap channel, its exit velocity is proportionally 5 times smaller.

3.2 Heat transfer

The heat generated at the windings is transferred by conduction to the stator. The flow field presented (Fig. 3a) receives the heat by convection from both windings and stator. Due the windings and stator thermophysical properties, the windings have virtually the same temperature (320 K) at its extension (Fig. 3b). Near the interface of the windings with the stator, a temperature drop of 10 K is observed. Along the stator radius, the temperature decreases evenly for the 5 stator blocks. This is an important information in an lumped model; it is necessary various points at the stator to represent this temperature gradient. At the middle radius of the stator, the stator temperature reaches the outlet air flow temperature. The air at the exit has its temperature increased in 10 K.

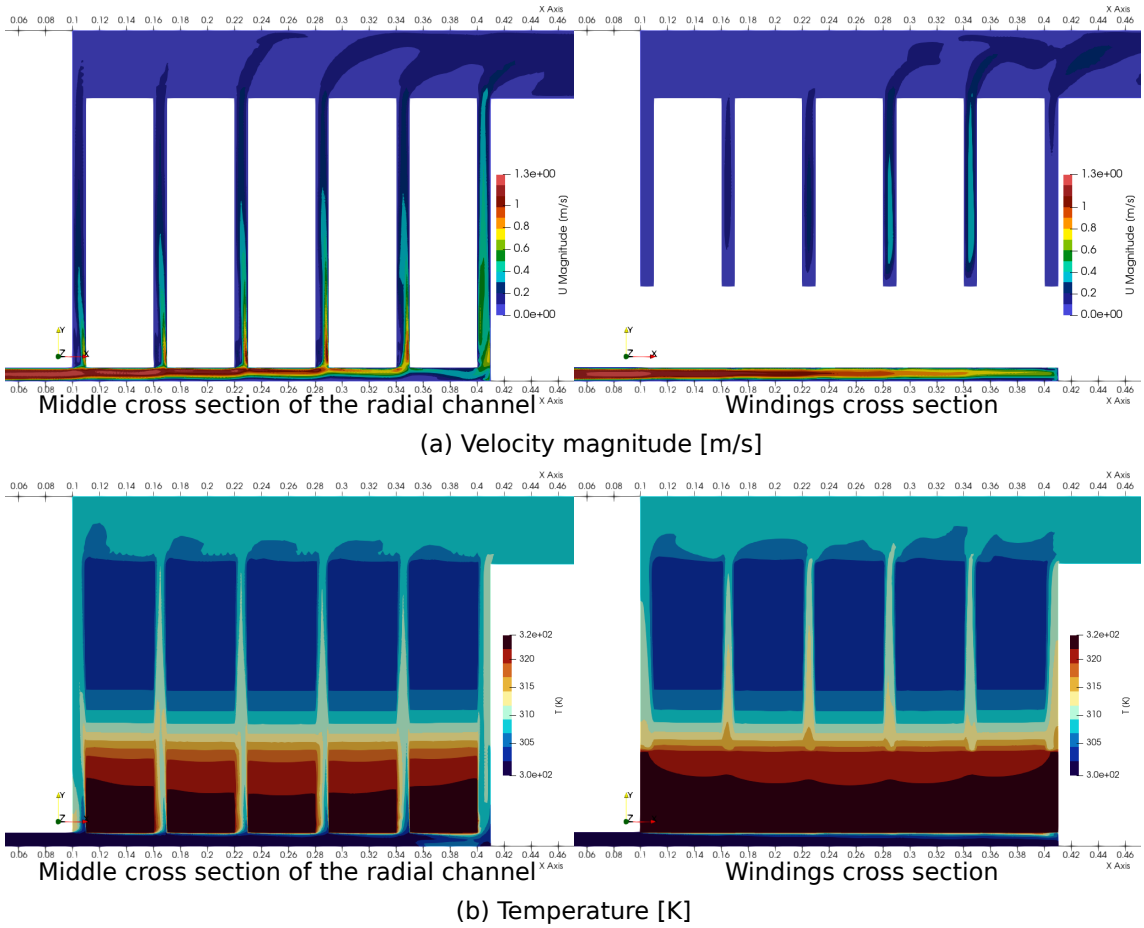

Figure 4. Velocity profiles at the air gap and stator channels

4 Conclusions

We have explored the flow behavior in a sequence of bifurcations that represents the flow in a stator of an electric machine. The main flow at the rotor-stator air gap is at the axial direction (Ux) and it was drawn to the radial channels. This scenario may change as rotational speed increases. In that case, the domain might be larger in the orthoradial direction. The highest temperature levels are at the windings and reached 320 K. Their temperature is near constant. The stator, in contrast, has a defined temperature gradient in the radial direction. It works as a fin for the windings, collaborating to the thermal energy transfer. The air temperature at the outlet is not negligible and reached 310 K.

Acknowledgements. The authors acknowledge the National Laboratory for Scientific Computing (LNCC/MCTI, Brazil), through the ambassador program (UFGD), subproject MNSE for providing HPC resources of the SDumont supercomputer, which have contributed to the research results reported within this paper. URL: http://sdumont.lncc.br.

Authorship statement. The authors hereby confirm that they are the sole liable persons responsible for the authorship of this work, and that all material that has been herein included as part of the present paper is either the property (and authorship) of the authors, or has the permission of the owners to be included here.

References

[1] D. Arumugam, P. Logamani, and S. Karuppiah. Electromagnetic & thermal analysis of synchronous generator with different rotor structures for aircraft application. *Alexandria Engineering Journal*, vol. 57, n. 3, pp. 1447–1457, 2018.

[2] A. Eme, R. Glises, D. Chamagne, J. M. Kauffmann, F. Chalon, and T. Péra. Thermal modelling for electrical machines fed with low voltage: First approach of a reliability model. *Math. Comput. Simul.*, vol. 71, n. 4, pp. 440–445, 2006.

[3] P. S. Ghahfarokhi, A. Kallaste, A. Belahcen, T. Vaimann, and A. Rassõlkin. Hybrid thermal model of a synchronous reluctance machine. *Case Stud. Therm. Eng.*, vol. 12, pp. 381–389, 2018.

[4] R. Khlissa, S. Vivier, G. Friedrich, K. El Kadri Benkara, and B. Assaad. Thermal modeling of an asymmetrical totally enclosed permanent magnet integrated starter generator. *Math. Comput. Simul.*, vol. 130, pp. 32–47, 2016.

[5] Z. Kolondzovski, A. Belahcen, and A. Arkkio. Multiphysics thermal design of a high-speed permanent-magnet machine. *Appl. Therm. Eng.*, vol. 29, n. 13, pp. 2693–2700, 2009.

[6] A. S. Bornschlegell, J. Pelle, S. Harmand, A. Fasquelle, and J.-P. Corriou. Thermal optimization of a high-power salient-pole electrical machine. *IEEE Transactions on Industrial Electronics*, vol. 60, n. 5, pp. 1734–1746, 2013.

[7] R. Wrobel and R. J. MGlen. Heat pipes in thermal management of electrical machines – A review. *Thermal Science and Engineering Progress*, vol. 26, pp. 101053, 2021.

[8] I. Ušakovs, D. Mishkinis, I. A. Galkin, A. Bubovich, and A. Podgornovs. Experimental thermal characterization of the in-wheel electric motor with loop heat pipe thermal management system. *Case Stud. Therm. Eng.*, vol. 47, pp. 103069, 2023.

[9] R. Wrobel. Analysis of power loss in heat pipes for integrated thermal management of next generation electrical machines. *Thermal Science and Engineering Progress*, vol. 47, pp. 102358, 2024.

[10] S. Lucas, S. Bari, R. Marian, M. Lucas, and J. Chahl. Cooling by Peltier effect and active control systems to thermally manage operating temperatures of electrical Machines (Motors and Generators). *Thermal Science and Engineering Progress*, vol. 27, pp. 100990, 2022.

[11] A. Selema, M. Beretta, M. Van Coppenolle, H. Tiismus, A. Kallaste, M. N. Ibrahim, M. Rombouts, J. Vleugels, L. A. I. Kestens, and P. Sergeant. Evaluation of 3D-Printed Magnetic Materials For Additively-Manufactured Electrical Machines. *J. Magn. Magn. Mater.*, vol. 569, pp. 170426, 2023a.

[12] A. Selema, M. Beretta, M. N. Ibrahim, J. Verwimp, M. Rombouts, J. Vleugels, L. A. I. Kestens, and P. Sergeant. Material Engineering of 3D-Printed Silicon Steel Alloys for the Next Generation of Electrical Machines and Sustainable Electromobility. *J. Magn. Magn. Mater.*, vol. 584, pp. 171106, 2023b.

[13] F. A. Kareem and P. A. Michael. An investigation on applications of additive manufacturing of electrical machines. *Mater. Today:. Proc.*, vol. 58, pp. 86–90, 2022.

[14] H. Wang, T. N. Lamichhane, and M. P. Paranthaman. Review of additive manufacturing of permanent magnets for electrical machines: A prospective on wind turbine. *Materials Today Physics*, vol. 24, pp. 100675, 2022.

[15] H. Tiismus, A. Kallaste, T. Vaimann, and A. Rassõlkin. State of the art of additively manufactured electromagnetic materials for topology optimized electrical machines. *Addit. Manuf.*, vol. 55, pp. 102778, 2022.

[16] C. C. T. Chow, M. D. Ainslie, and K. T. Chau. High temperature superconducting rotating electrical machines: An overview. *Energy Rep.*, vol. 9, pp. 1124–1156, 2023.

[17] I. B. Celik, U. Ghia, P. J. Roache, C. J. Freitas, H. Coleman, and P. E. Raad. Procedure for estimation and reporting of uncertainty due to discretization in cfd applications. *Journal of fluids engineering*, vol. 130, n. 7, pp. 78001, 2008.

[18] C. Greenshields and H. Weller. *Notes on Computational Fluid Dynamics: General Principles*. CFD Direct Ltd, Reading, UK, 2022.